PNAS
www.pnas.org

Supplementary Information for

Empirical evidence for stability of the 405 kyr Jupiter-Venus eccentricity cycle over hundreds of millions of years

Dennis V. Kent[1,2]
Paul E. Olsen[2]
Cornelia Rasmussen[3]
Christopher Lepre[1,2]
Roland Mundil[4]
Randall B. Irmis[3,5]
George E. Gehrels[6]
Dominique Giesler[6]
John W. Geissman[7]
William G. Parker[8]

[1]Earth & Planetary Sciences, Rutgers University, Piscataway, NJ 08854
[2]Lamont-Doherty Earth Observatory of Columbia University, Palisades, NY 10964
[3]Department of Geology & Geophysics, University of Utah, Salt Lake City, UT 84112
[4]Berkeley Geochronology Center, 2455 Ridge Rd., Berkeley CA 94709
[5]Natural History Museum of Utah, University of Utah, Salt Lake City, UT 84108
[6]Department of Geosciences, University of Arizona, Tucson, AZ 85721
[7]Department of Geosciences, University of Texas at Dallas, Richardson, TX 75080
[8]Petrified Forest National Park, Petrified Forest, AZ 86028

Corresponding author: Dennis Kent
Email: dvk@rutgers.edu

This PDF file includes:

Supplementary Text

PFNP-1A core logistics and sampling

Core CPCP-PFNP-13-1A (henceforth PFNP-1A) was drilled in the parking lot at Chinde Point in the northern part of the Petrified Forest National Park (35.085933° N, 109.795500° W, WGS84 datum) in November and December, 2013, by Ruen Drilling, Inc. The HQ core hole configuration was designed to be inclined 60° from horizontal (to facilitate orientation of cores in the flat-lying beds) at an azimuth of 135° (to avoid a late Cenozoic Bidahochi lava feeder dike). EZ Shot data collected during drilling give core hole inclinations ranging from 58.3° - 62.0° and azimuths (true north) from 132.2° - 140.3°, conforming to the design specifications. Accordingly, we use an inclination of 60° and azimuth of 135° to reorient samples taken from the core. The drilled interval had a total core length of 519.9 m (450.0 m stratigraphic equivalent assuming the hole was inclined at 60° and beds are horizontal). The 6.25-cm-diameter core was collected in 395 runs, each nominally 1.5 m long. Each run was cut into two to three segments (each not exceeding 76.2 cm for scanning purposes) for a total of 931 sections. Orientation of each core run was performed using the Reflex ACT II(III) device. A video of how this device works and how the data are transferred to the core is at: http://www.youtube.com/user/reflexinstruments, with the relevant video being: https://www.youtube.com/watch?v=FrPKM-_D72A.

The core orientation information was transferred from the device to the bottom of each core. Core in its liner was transferred to the onsite LacCore tent where a white line was drawn from the orientation mark along the core axis length before being sliced into core segments. The white line is consistent for all cores, and always on the down-side of the core opposite from the azimuth of the inclined drilled hole. The up/down orientation of the core segments is maintained with blue endcaps on tops and red endcaps on bottoms of liners. In a small proportion of cases the orientation is ambiguous or reversed due to a bad orientation device reading (one of the two devices was not working for a period of time), the core rotating inside the plastic liner, or possibly due to operator error during core cutting and labeling in the lab. At LacCore, the core segments were split along the white line up with a 12” diameter diamond saw lubricated with water. After scanning and description, the work-halves of the cores were shipped to the Rutgers Core Repository. Looking down the borehole, the work halves of the cores would be on the observer’s left side, i.e., the northeast half of the core with the split face toward the southwest.

Sediments above the Sonsela Mb. in the core were generally too poorly indurated to take standard 2.5 cm-diameter plugs with a water-cooled diamond drill bit. An initial suite of samples was thus taken mostly by plucking loose pieces from the split face of the working-halves of the cores. The subsequent and preferred method of sampling to obtain coherent material was to cut half-round or quarter-round slices about 2 cm thick, sometimes through the plastic liner, using a bandsaw with a carborundum-tipped blade. Specimens for paleomagnetic measurements were prepared by cutting a flat surface on the up-core side and a perpendicular flat surface parallel to the split-face of the core. The split-face sample surface was inscribed with an arrow marking the up-core direction on what should be an oriented face as determined from the Reflex device. Fine-grained reddish-colored sediment was preferentially sampled although this lithology was often associated with massive paleosols that had few indictors of bedding; silt- and sand-sized sediment with layering and oblate bleached haloes around organic blebs or minerals (with major axes assumed parallel to bedding) were sometimes present in the same core run and such indicators of bedding provided an independent check on the orienting tool. Given the known azimuth and dip of the drill core, traces of bedding that are horizontal *in situ* should appear to tilt 30° down to the right looking at the split face of the working-halves of the core, for the interval studied here.

Background information on core PFNP-1A can be found at http://www.ldeo.columbia.edu/~polsen/cpcp/CPCP_Scientific_Drilling.html.

Paleomagnetic analyses

Backfield demagnetization curves of isothermal remanent magnetization (IRM) show that the magnetizations of the sampled units are typically dominated by hematite, as indicated by lack of saturation in 2.5 T fields and high remanent coercivities of about 700 mT, with some contributions of a lower coercivity phase like magnetite that even become dominant in some of the pale-colored sandstones of the BFB (**Fig. S1**). Accordingly, progressive thermal demagnetization was used to isolate the characteristic component of the natural remanent magnetization (NRM) of each specimen. Samples were heated at temperature for 45 minutes in a ASC TD48 oven in typically 12 steps from 100° (or 150°) to 675°C and the magnetizations after each step were measured after cooling to room temperature in a 2G Model 760 3-axis DC SQUID magnetometer, all housed in a magnetically-shielded room at LDEO.

Vector endpoint demagnetograms (**Fig. S2**) typically show the removal of a spurious (not systematically oriented) low unblocking temperature component to 300°C followed in most samples by a stable component with shallow inclination up to 675°C. A least-squares linear fit using principal component analysis over the 3 to 7 (typically 5) demagnetization steps in the range 300°–600°C and anchored to the origin was used to assess the characteristic remanent magnetization (ChRM) in each sample. The 132 sample characteristic remanent magnetizations (ChRM) that were deemed acceptable based on progressive thermal demagnetization (maximum angular deviation (MAD) (1)) of 16° or less (average MAD 8°) are quite scattered but generally fall into two populations (**Fig. S3**), a northerly-directed group (Dec=0.4°, Inc=+22.7°, a95=6.0°, k=7.1, n=90) and a southerly-directed group (Dec=172.8°, Inc=+8.1°, a95=12.5°, k=4.1, n=42). The declinations are close to 180° apart but there is a downward bias in the inclinations so the two populations are not antipodal (departure=32±14°) and do not pass a reversal test (2). The overall mean direction after inverting the southerly population is Dec=358.1°, Inc=+13.8°, a95=6.1°, k=5.0 for n=132 samples. The ChRM of approximately equivalent strata in outcrop had essentially the same mean direction (Dec=358.9° Inc=+8.2°) although with considerably less scatter (a95=2.8°, k=33.8 for n=53 samples from Painted Desert Mb., equivalent to Petrified Forest Mb. here) and passed a reversal test (Table 1 in (3)). The expected direction for the core site locality using the 210 Ma reference pole for North America (64.2°N 91.2°E A95=2.9°)(4) is Dec=350.9° Inc=20.6°, corresponding to a paleolatitude of 10.7°N±2.9°. The shallower than expected mean ChRM direction of the upper Chinle in core PFNP-1A (and in outcrop (3)) can be attributed to sedimentary inclination error corresponding to a flattening factor of ~0.7, typical of many Triassic continental redbeds with early-acquired magnetizations (5). The accepted sample data were used to construct a paleomagnetic polarity sequence for the upper 280 mcd of core PFNP-1A (**Tables S2, S3**).

U-Pb CA-TIMS analytical procedures

The samples were crushed and mineral concentrates were then purified using standard mineral separation techniques, including sieves, magnetic separation and density separation at the

LaserChron Center at University of Arizona, mounted on epoxy disks and polished to about one-half of the crystal width followed by LA-ICPMS analyses providing a survey of the range of zircon ages present. At the Berkeley Geochronology Center (BGC) 20-30 crystals displaying the youngest LA-ICPMS age from each sample were extracted from the mount and prepared for zircon U-Pb CA-TIMS (Chemical Abrasion-Thermal Ionization Mass Spectrometry). Prior to TIMS analysis all zircons were pretreated using thermal annealing at 850°C for 48 hrs, followed by chemical abrasion with concentrated HF in pressurized dissolution capsules at 220°C for 8 to 12 hrs. Complete dissolution in an ultraclean wet chemistry laboratory was preceded by cleaning the crystals in ultrasonically agitated aqua regia followed by multiple steps of rinsing in clean HNO_3. Zircon crystals were then spiked with ^{205}Pb-^{233}U- ^{235}U tracer solution (both a solution mixed and calibrated at BGC as well as Earthtime 535 tracer were used; for intercalibration see Ref. (6)), and then dissolved by vapor transfer in HF using miniature PTFE capsules at 220°C for 6 days. After dissolution, the equilibrated sample/tracer solution was loaded on zone refined Re filament using silica gel as emitter substance (7). Isotope ratios were determined on a Micromass Sector 54 mass spectrometer using a Daly-type ion counter positioned behind a WARP filter. Pb (as Pb^{+}) and U (as UO^{2+}) were run sequentially on the same filament (for calibration of the BGC tracer see (6, 8, 9)). Repeat measurements of the total procedural blank averaged 0.82 ± 0.36 pg Pb (U blanks were indistinguishable from zero), with ^{206}Pb/^{204}Pb = 18.40 ± 0.46, ^{207}Pb/^{204}Pb = 15.64 ± 0.25, ^{208}Pb/^{204}Pb = 38.04 ± 0.75 (all 2σ of population), and a ^{206}Pb/^{204}Pb-^{207}Pb/^{204} Pb correlation of +0.47 (ratios and uncertainties were propagated into the age and age-error calculations). The total procedural blank including ion exchange chemistry is also as low as 1 pg but scatter in total common Pb concentration and possibly common Pb composition suggests that results from unextracted analyses of zircon yield better reproducibility. Deficient radiogenic ^{206}Pb in zircon due to initial deficit of ^{230}Th is accounted for by assuming a partition coefficient ratio DTh/DU of 0.2 (as applied in (10)), or by assuming Th/U in the parent magma to be 3.5 where the ET535 tracer solution was used (the resulting difference in age from either approach is negligible). Mass fractionation of U during analysis was controlled by the U double spike, whereas Pb mass fractionation was corrected by 0.15 ± 0.6 %/AMU (based on multiple analyses of NBS 981).

U-Pb CA-TIMS results

The analytical data of four samples from the Chinle Fm subjected to U-Pb zircon CA-TIMS analyses (**Fig. S4**) are presented below. The ages are considered maximum depositional ages because the zircons contained in the deposits are redeposited and the lag between the ages of juvenile volcanic zircons and deposition is unknown but arguably short or not even resolvable. Therefore ages reported here, which serve to constrain the ages of corresponding polarity zones in the Late Triassic of the Colorado Plateau and the astronomically calibrated Newark Hartford basin, are not considered to represent accurate depositional ages by themselves.

Ages are reported as weighted mean ^{206}Pb/^{238}U ages (with uncertainties at the 95% confidence level) unless stated otherwise **(Tables S4, S5)**.

Sample 52Q-2 from 56.0 ± 0.08 msd is a fine-grained white sandstone from the Black Forest Bed within the upper part of the Petrified Forest Mb. in polarity zone PF2r. An age of 210.08 ± 0.22 Ma (MSWD = 0.82) can be calculated from a coherent cluster of 6 out 14 analyses. Seven older analyses range from 210.52 to 214.92 Ma, and one age is resolvably younger at 203.06 Ma and likely compromised by Pb loss. Th/U in this sample ranges from 0.38 to 1.97, which suggests, due to the wide range, that the crystals are derived from various sources. Our age of 210.08 ± 0.22 Ma is in agreement with an age of 209.926 ±0.072 Ma reported for the Black Forest Bed, but not necessarily from exactly the same stratigraphic level. PF2r correlates with E16r with an astronomically tuned age range from 209.9 to 210.2 Ma.

Sample 158Q-2 is a sandstone from 172.0 ± 0.09 msd in the uppermost Sonsela Mb. and the middle portion of polarity zone PF4n. $^{206}Pb/^{238}U$ ages of 17 zircon analyzed range from 207.88 to 223.82 Ma, but ages <210 Ma are not feasible because of stratigraphic and age constraints from sample 52Q-2 9 (see below). We therefore conclude that at least the youngest 4 analyses of 158Q-2 suffered Pb loss despite an aggressive pretreatment of chemical abrasion. A cluster of nine analyses yields an age of 213.55 ± 0.28 Ma, however, the MSWD is elevated (2.0) suggesting that a subset of this cluster is representative of the maximum depositional age (either 213.00 ± 0.36 Ma or 213.71 ± 0.20 Ma if Pb loss is more severe). Th/U in the sample ranges from 0.70 to 1.66. Polarity zone PF4n correlates with E15n from the Newark Hartford basin with a predicted age from 212.6 to 213.4 Ma.

Sample 177Q-1 from 190.0 ± 0.09 msd is stratigraphically lower from the upper Sonsela Mb and also from within polarity zone PF4r. The $^{206}Pb/^{238}U$ ages are dispersed and range from 212.81 to 216.37 Ma with Th/U ranging from 0.64 to 1.85 (the latter can perhaps be considered an outlier). Some of the ages are also compromised by imprecision due to very small sample size. At face value the youngest age of 212.81 ± 1.25 Ma must be considered a maximum depositional age if Pb loss can be excluded. Because none of the ages were convincingly reproduced, the latter age is ambiguous.

Sample 182Q-1 from 195.3 ± 0.13 msd is a mud/siltstone from the upper Sonsela Mb. that was dated to an age of 214.08 ± 0.20 Ma (MSWD = 1.02) based on the youngest 6 analyses. Five additional analyses from selected crystals range from 214.88 to 219.54 Ma. Th/U of the crystals from the coherent cluster ranges from 0.49 to 1.05. Sample 182Q-1 is from within polarity zone PF4r which, based on the correlation with the APTS, is equivalent to polarity zone E14r (213.4 to 214.9 Ma).

Correlation of samples from core PFNP-1A and outcrop composite section

The BFB is a distinctive, white tuffaceous crossbedded sandstone that can be traced over large areas of the PFNP. Moreover, it was sampled for dating (11) in outcrop at Chinde Point, the same area as the drilling site for PFNP-1A, making its correlation to the core secure. In contrast, other dated horizons reported from the Sonsela Mb. (as well as the Blue Mesa and Mesa Redondo Members that are not considered here) of the Chinle Fm. (11-13) are from less distinctive beds sampled over a wide geographic area and thus present more of a challenge tying them into PFNP-1A. We use a lithostratigraphic composite section measured for the Chinle Fm. in outcrop (11, 12) as a framework for the U-Pb dates from outcrop samples. There is actually a remarkably good correlation between the cumulative thickness of lithostratigraphic subdivisions of the Chinle Fm. measured in outcrop and their stratigraphic thicknesses in core PFNP-1A, with a coefficient of determination, R^2>0.99 (**Fig. S5; Table S1**). We use the regression from the base of the Sonsela Mb. to the base of the Owl Rock Mb. pinned to the common base of the BFB to place the U-Pb CA-TIMS zircon data from outcrops analyzed by the MIT lab of the BFB and the Sonsela Mb. (11, 13) into the common lithostratigraphic depth scale for comparison with the U-Pb CA-TIMS zircon data analyzed by the BGC lab and reported here from core PFNP-1A (**Table S4**). Depth relationships of the MIT outcrop samples and the BGC core sample data are very similar (**Fig. S6**). Given the added stratigraphic uncertainties of projecting the MIT outcrop dates to PFNP-1A, we prefer to use the BGC dates taken from the core (samples 52Q2, 158Q2 and 182Q1), which provide a linear regression (msd in core PFNP-1A = 34.34 * Age - 7158, R^2=0.999) that turns out to be remarkably close to a regression of predicted stratigraphic depth versus ages from the APTS via magnetostratigraphy (msd in core PFNP-1A = 34.84 * Age - 7258, R^2=0.985) (**Fig. 3**).

The high level of agreement between the APTS and U-Pb CA-TIMS dates, which shows that hiatuses are not apparent in the APTS, offers a unique opportunity to test the accuracy of the detrital zircon ages in terms of age bias due to redeposition. A linear fit with such high correlation of determination (R^2>0.99) to the CA-TIMS zircon ages suffices because, a priori, the magnitude of age bias due to redeposition is not known. However, some of this bias could be estimated from the departures of zircon ages from the APTS ages, if assumed to be accurate. For example, application of the StalAge algorithm with a Monte Carlo technique (14) to the verified APTS ages (**Fig. S7**) reveals small-scale offsets from a linear age-depth relationship that are most likely due to varying age biases in the populations of redeposited zircons. Such an approach might be useful to extract depositional ages from large populations of LA-ICPMS detrital zircon dates.

References

1. Kirschvink JL (1980) The least-squares line and plane and the analysis of palaeomagnetic data. *Geophysical Journal of the Royal Astronomical Society* 62:699-718.
2. McFadden PL & McElhinny MW (1990) Classification of the reversal test in palaeomagnetism. *Geophysical Journal International* 103:725-729.
3. Steiner MB & Lucas SG (2000) Paleomagnetism of the Late Triassic Petrified Forest Formation, Chinle Group, western United States: Further evidence of "large" rotation of the Colorado Plateau. *Journal of Geophysical Research* 105:25,791-725,808.
4. Kent DV & Irving E (2010) Influence of inclination error in sedimentary rocks on the Triassic and Jurassic apparent polar wander path for North America and implications for Cordilleran tectonics. *Journal of Geophysical Research* 115:B10103, doi:10110.11029/12009JB007205.
5. Kent DV & Tauxe L (2005) Corrected Late Triassic latitudes for continents adjacent to the North Atlantic. *Science* 307:240–244.
6. Irmis RB, Mundil R, Martz JW, & Parker WG (2011) High-resolution U–Pb ages from the Upper Triassic Chinle Formation (New Mexico, USA) support a diachronous rise of dinosaurs. *Earth and Planetary Science Letters* 309:258-267.
7. Gerstenberger H & Haase G (1997) A highly effective emitter substance for mass spectrometric Pb isotope ratio determinations. *Chemical Geology* 136(3-4):309-312.
8. Mundil R, Ludwig KR, Metcalfe I, & Renne PR (2004) Age and timing of the Permian mass extinctions: U/Pb dating of closed-system zircons. *Science* 305:1760-1763.
9. Black LP*, et al.* (2003) The application of SHRIMP to Phanerozoic geochronology; a critical appraisal of four zircon standards. *Chemical Geology* 200(1-2):171-188.
10. Wotzlaw J-F*, et al.* (2014) Towards accurate numerical calibration of the Late Triassic: High-precision U-Pb geochronology constraints on the duration of the Rhaetian. *Geology* 42(7):571-574.
11. Ramezani J*, et al.* (2011) High-precision U-Pb zircon geochronology of the Late Triassic Chinle Formation, Petrified Forest National Park (Arizona, USA): Temporal constraints on the early evolution of dinosaurs. *Geological Society of America Bulletin* 123(11/12):2142-2159.
12. Atchley SC*, et al.* (2013) A linkage among Pangean tectonism, cyclic alluviation, climate change, and biologic turnover in the Late Triassic: The Record From The Chinle Formation, Southwestern United States. *Journal of Sedimentary Research* 83:1147-1161.
13. Nordt L, Atchley S, & Dworkin S (2015) Collapse of the Late Triassic megamonsoon in western equatorial Pangea, present-day American Southwest. *Geological Society of America Bulletin* 127:1798-1815.
14. Scholz D & Hoffmann DL (2011) StalAge – An algorithm designed for construction of speleothem age models. *Quaternary Geochronology* 6:369–382.
15. Martz JW & Parker WG (2010) Revised Lithostratigraphy of the Sonsela Member (Chinle Formation, Upper Triassic) in the Southern Part of Petrified Forest National Park, Arizona. *PLoS ONE* 5(2):e9329.
16. Olsen PE*, et al.* (2018) Colorado Plateau Coring Project, Phase I (CPCP-I): A continuously cored, globally exportable chronology of Triassic continental environmental change from Western North America. *Scientific Drilling* in review.
17. Kent DV, Olsen PE, & Muttoni G (2017) Astrochronostratigraphic polarity time scale (APTS) for the Late Triassic and Early Jurassic from continental sediments and correlation with standard marine stages. *Earth-Science Reviews* 166:153–180.

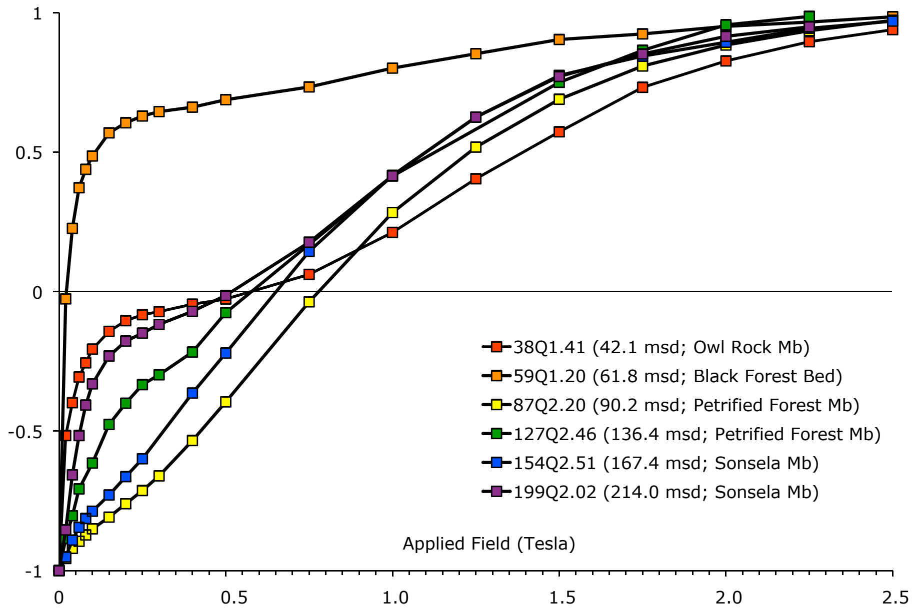

Fig. S1. Normalized backfield isothermal remanent magnetization (IRM) demagnetization curves of representative samples from the upper Chinle Formation (Owl Rock, Petrified Forest and Sonsela members) in core PFNP-1A.

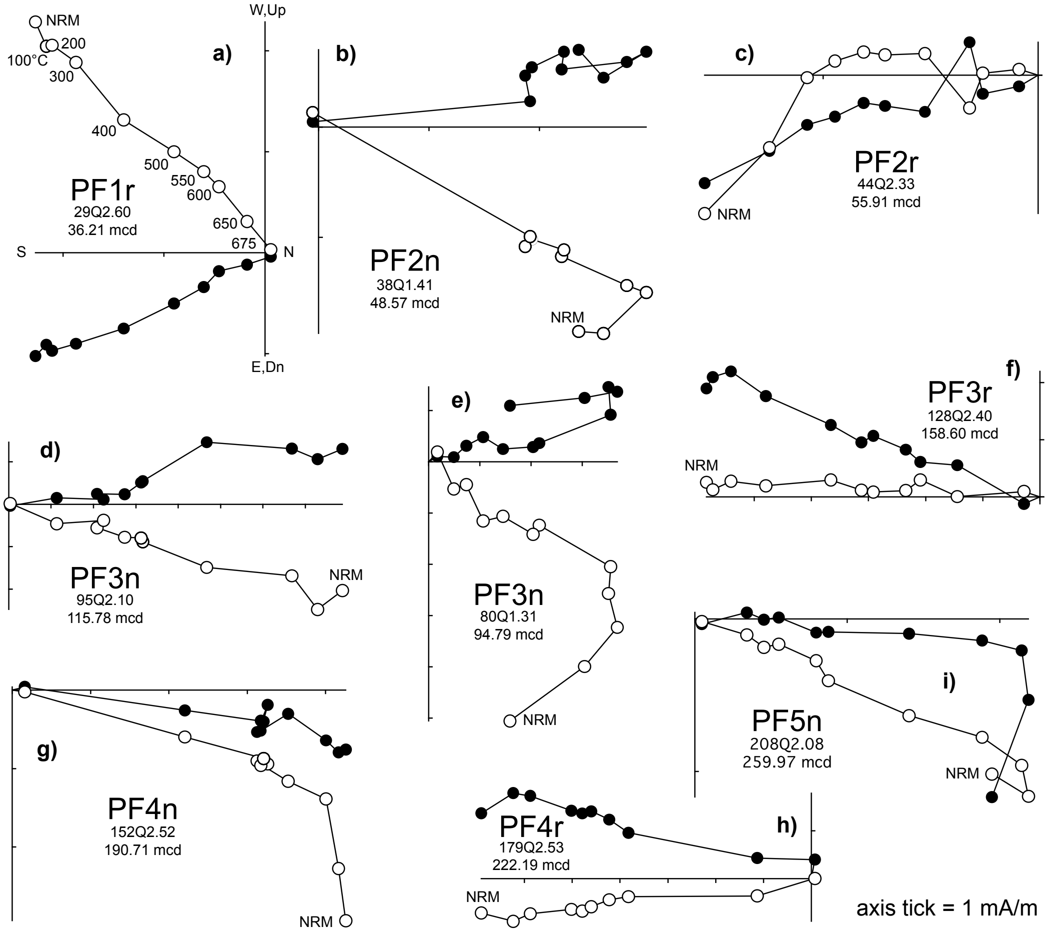

Fig. S2. Vector endpoint demagnetograms of NRM for representative samples from upper Chinle Formation in core PFNP-1A. All plots (a–i) use same convention as for sample in upper left (a) with open/closed symbols on vertical/horizontal orthogonal axes in stratigraphic coordinates (corrected for azimuth and tilt of core hole). NRM is natural remanent magnetization of the sample before stepwise thermally demagnetization with levels in °C as labeled in (a).

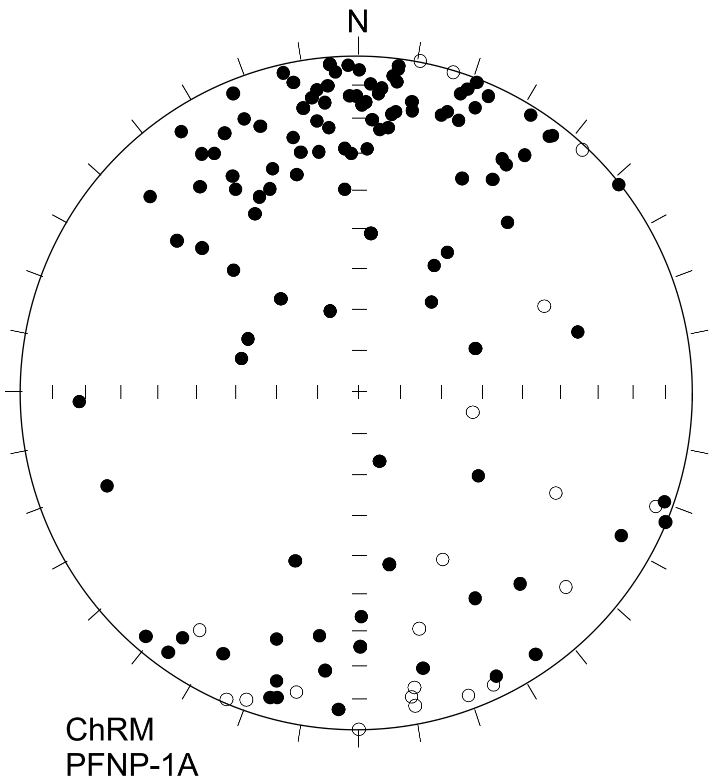

Fig. S3. Equal-area plot (open/closed circles on upper/lower hemisphere) of ChRM directions isolated in 132 samples from upper Chinle Fm. in core PFNP-1A (**Table S3**). The ChRM directions fall into a northerly group interpreted as normal polarity and a southerly group of reverse polarity.

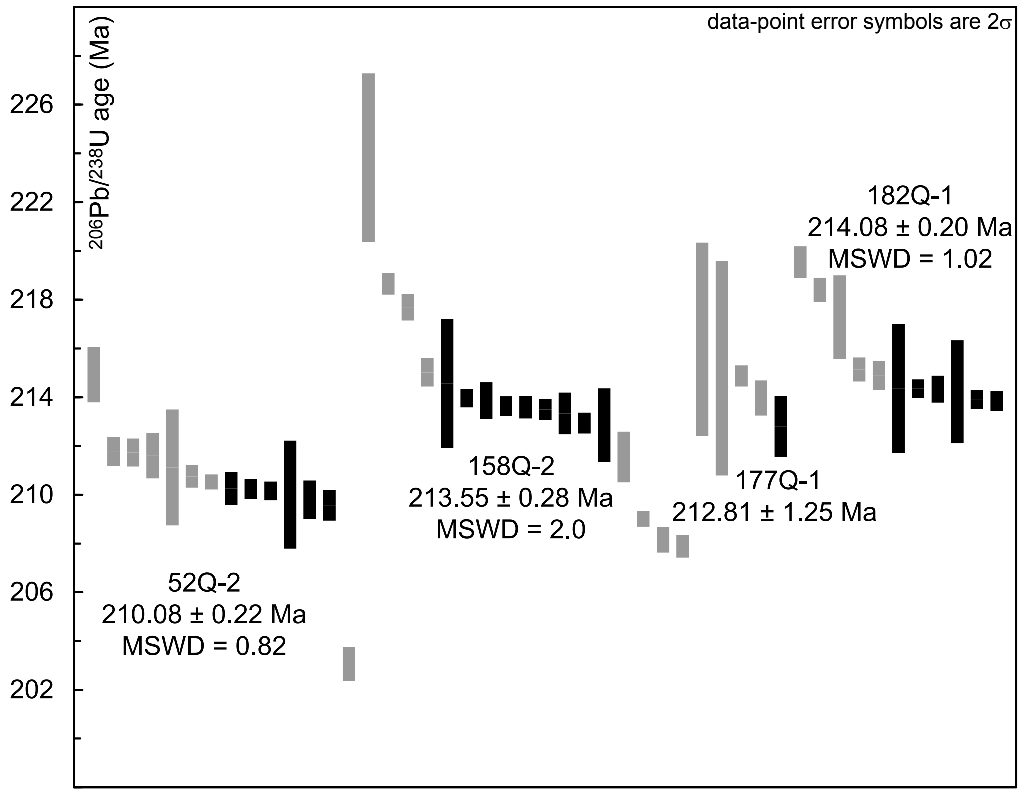

Fig. S4. Individual 206Pb/238U ages of zircon analyses from samples of tuffaceous sandstones in Chinle Fm. from core PFNP-1A (see **Table S4).** Vertical bars show full 2σ uncertainties; zircon analyses with black bars were used to calculate the sample mean age and 2σ uncertainty (95% confidence interval).

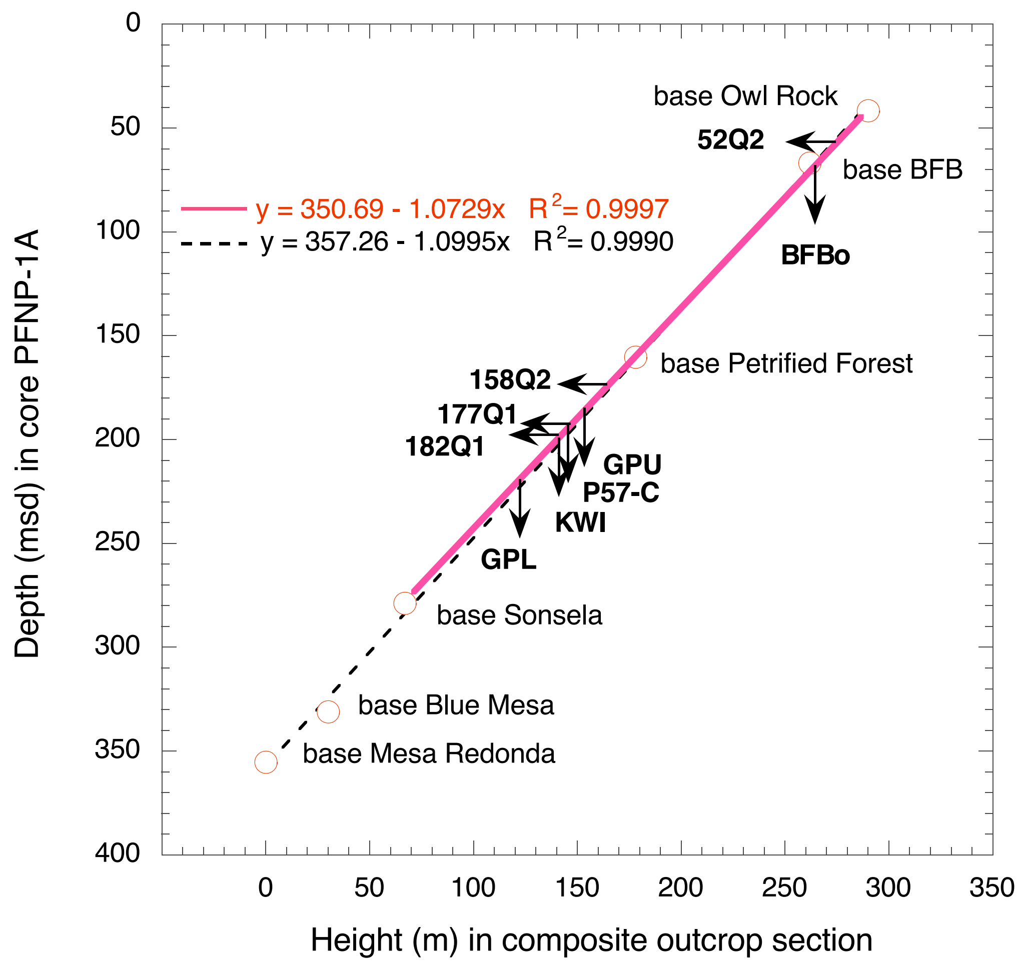

Fig. S5. Stratigraphic heights (circles) of the bases of the Mesa Redonda, Blue Mesa, Sonsela, Petrified Forest and Owl Rock members including the base of the Black Forest Bed (BFB) of the Chinle Fm. identified in a composite outcrop section (11, 12) versus their depth in core PFNP-1A (**Table S1**). Two linear regressions are shown (both equations given), one for all these units (dashed line) and another for just the base of the Sonsela Mb. to the base of the Owl Rock Mb. (solid line), which was used to place the U-Pb CA-TIMS dated zircon samples from outcrop (BFBo, GPU, P57-C, KWI and GPL from (11, 13)) in the same stratigraphic framework as the U-Pb CA-TIMS dated zircon samples from core PFNP-1A (52Q2, 158Q2, 177Q1, and 182Q1 reported here) (**Table S4**).

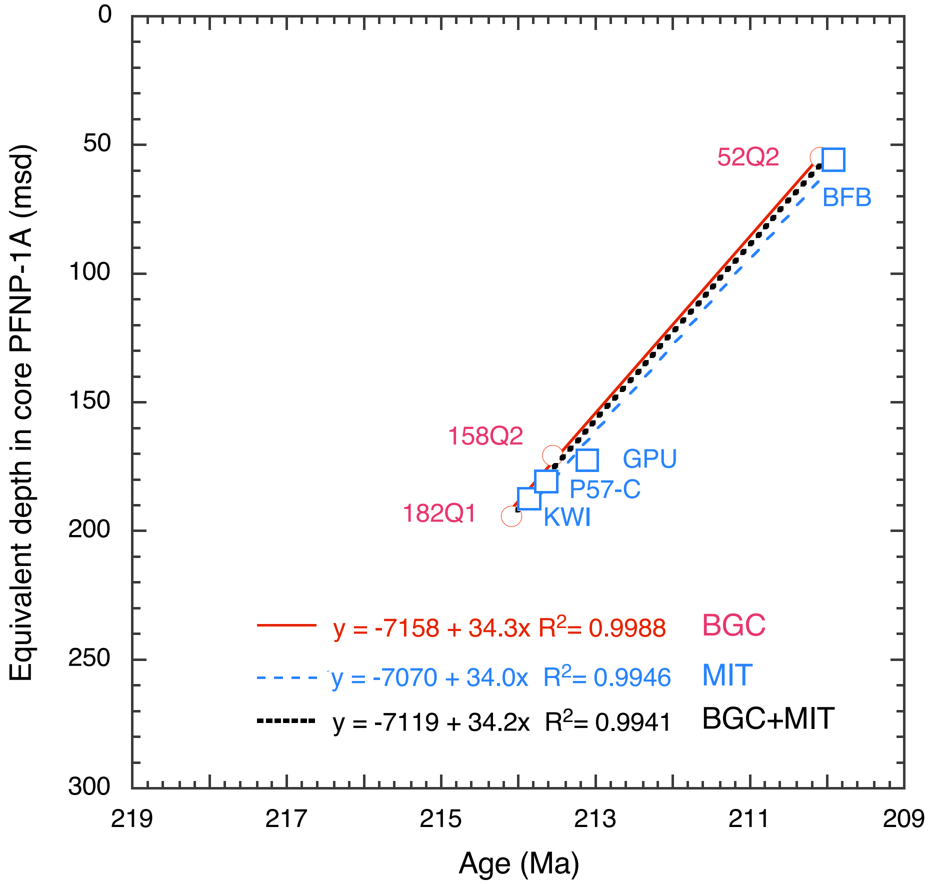

Fig. S6. Stratigraphic distribution of U-Pb CA-TIMS dated zircon samples taken from core PFNP-1A and analyzed by the BGC lab and reported here (circles; sample 177Q1 with large uncertainty of ±1.25 Myr is not plotted) compared to published U-Pb CA-TIMS dated zircon samples taken from outcrop (squares) and analyzed in the MIT lab (11, 13) that were projected into the depth scale of the core using base of the BFB in common (**Table S4**). Linear regressions of depth versus age for both sets of data separately and combined are shown.

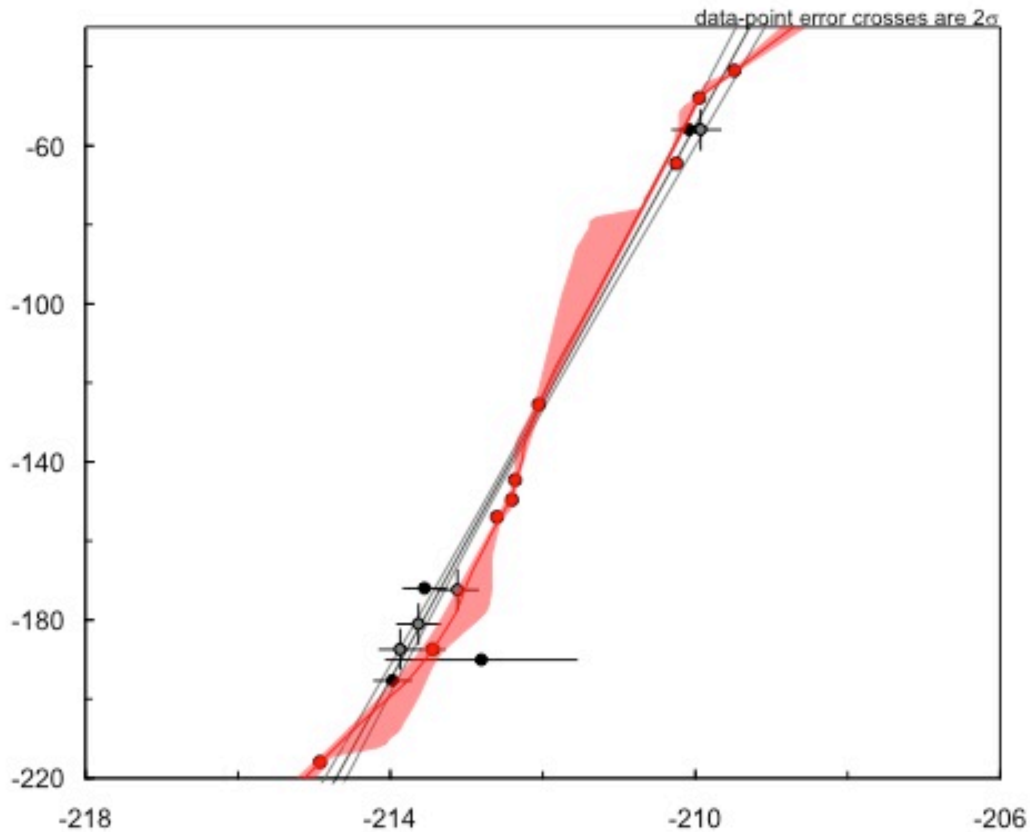

Fig. S7. Stratigraphic distribution of U-Pb CA-TIMS dated samples taken from core PFNP-1A (circles) and published results taken from outcrop (11, 13) that were projected into the common depth scale of the core with an assumed ±5 m stratigraphic uncertainty (squares), all shown with ±2σ age uncertainties (**Table S4**), compared with magnetozone boundaries with their stratigraphic uncertainties in core PFNP-1A as correlated to APTS (**Table S2**). The 95% confidence interval in the depth versus age relationship for the magnetozones using the StalAge algorithm and Monte Carlo technique (14) overlaps for the most part with a linear fit and 95% error envelope through the zircon ages but reveals varying age biases in the populations of redeposited zircons.

Table S1. Lithostratigraphic subdivisions of Chinle Fm. in core PFNP-1A compared to their relative position in a composite outcrop section in and around Petrified Forest National Park.

Rock units[&]	PFNP-1A, msd[#]	Composite height, m*
top (eroded) of Chinle Fm.	20.6	
base Owl Rock Mb.	41.7	290.0
base Black Forest Bed	66.9	262.0
base Petrified Forest Mb.	160.3	178.0
base Sonsela Mb.	278.9	67.0
base Blue Mesa Mb.	331.2	30.0
base Mesa Redonda Mb. (=base Chinle Fm.)	355.4	0.0

[$]Ref. (15). [#]Meters stratigraphic depth for a core hole inclination of 60°; Ref. (16). *Ref. (12).

Table S2. Paleomagnetic polarity zones in core PFNP-1A.

Magneto-zone	Base, mcd	Base, msd	±, msd	Chron	Age, Ma	Ecc_{405}: k
PF1r	47.40	41.05	0.41	E17r	209.49	517.73
PF2n	55.40	47.98	0.44	E17n	209.95	518.87
PF2r	74.49	64.51	2.70	E16r	210.25	519.60
PF3n	144.80	125.40	1.65	E16n	212.05	524.05
PF3r.1r	166.80	144.45	0.55	E15r.2r	212.36	524.82
PF3r.1n	172.60	149.48	1.63	E15r.1n	212.40	524.90
PF3r	177.67	153.87	0.48	E15r	212.60	525.41
PF4n	216.23	187.26	5.16	E15n	213.44	527.47
PF4r	249.10	215.73	1.77	E14r	214.92	531.15
PF5n	>278.01	>240.76		E14n?	216.16	534.19

Magnetozone is the magnetic polarity interval numbered from the uppermost identifiable polarity interval of the Chinle Fm. in this core (PF1r) to the lowermost polarity interval (PF5n) in the part of the core sampled for this study, with a prefix, PF, for Petrified Forest and suffixes n and r for predominantly normal and reverse polarity. The identified base of each magnetozone is designated in mcd, meters core depth, and in msd, meter stratigraphic depth, msd, by taking into account 60° inclination of the core hole; sampling resolution for polarity boundary given as ± msd (**Table S4**). Proposed correlative Chron for each magnetozone is given with its starting Age in million years ago (Ma) and position within a 405 kyr orbital eccentricity cycle (Ecc_{405}:k) where k is the fractional number of predicted cycles counting back from the most recent peak value (k=1) at 0.216 Ma (17). Reliable data for PF1r start in samples only at 38 mcd (~33 msd) above which the results are very scattered due to weathering and drilling disturbance in the porous poorly lithified sediment; the base of PF5n was not reached in this suite of samples.

Table S3. Paleomagnetic results from principal component analysis.

mcd	msd/60°	ID	N	MAD	bDec	bInc	bLon	bLat	rbLon	rbLat	T1	T2	Notes
24.03	20.81	20Q2.44	5	12.7	319.9	60.6	184.2	58.2	218.0	48.9	300	600	
29.28	25.36	24Q1.33	5	24.5	110.0	-9.5	332.4	-19.1	343.3	-29.5	300	600	
29.78	25.79	24Q2.05	5	3.7	100.2	-61.9	14.2	-29.9	26.2	-21.3	300	600	
30.61	26.51	25Q1.13	5	13.7	20.9	2.3	35.8	50.9	359.5	58.7	300	600	
31.75	27.50	25Q2.64	5	3.7	125.2	54.3	292.4	-3.4	295.2	-27.3	300	600	
32.22	27.90	26Q2.06	5	7.5	16.6	15.7	37.0	58.9	347.6	64.5	300	600	
33.34	28.87	27Q1.58	5	8.2	69.7	59.8	312.0	36.2	304.4	15.4	300	600	
33.91	29.37	27Q2.59	5	7.8	155.3	-5.0	290.9	-50.2	317.1	-72.5	300	600	
34.50	29.88	28Q2.18	5	13.2	111.1	-6.2	330.3	-19.0	341.2	-30.3	300	600	
36.21	31.36	29Q2.60	5	3.5	153.4	-43.7	324.8	-65.2	28.1	-67.8	300	600	
36.90	31.96	30Q1.63	5	13.8	118.7	12.3	317.6	-19.2	328.2	-35.4	300	600	
37.39	32.38	30Q2.55	5	3.8	268.0	18.2	169.0	3.7	171.8	8.7	300	600	
38.04	32.94	31Q1.55	5	7.5	249.5	21.4	181.3	-9.8	177.0	-8.9	300	600	
38.64	33.46	31Q2.44	5	10.5	146.0	7.0	296.9	-39.9	315.3	-61.5	300	600	
41.00	35.51	33Q1.62	5	35.8	83.5	1.5	343.3	5.7	342.6	-2.4	300	600	
42.53	36.83	34Q2.51	5	11.3	26.3	24.7	16.6	57.5	336.4	55.3	300	600	high J?
42.10	36.46	34Q2.08	5	9.8	200.6	45.6	230.0	-24.9	217.0	-42.5	300	600	
42.93	37.18	34Q3.18	5	9.9	170.0	46.9	260.0	-26.1	255.1	-51.2	300	600	
42.95	37.20	34Q3.20	5	6.9	166.9	17.1	268.5	-44.5	265.5	-70.5	300	600	
43.83	37.96	35Q1.31	5	10.7	163.5	72.5	258.9	3.9	258.0	-21.3	300	600	
44.39	38.44	35Q2.15	4	8.5	139.9	26.6	295.2	-27.9	305.6	-50.6	300	550	
45.20	39.14	36Q1.09	5	11.5	117.2	-34.6	341.5	-32.8	359.7	-37.6	300	600	
45.29	39.22	36Q1.18	4	5.8	215.7	11.3	203.4	-37.2	181.9	-42.5	300	550	
46.10	39.92	36Q2.35	5	32.2	224.2	39.0	207.0	-19.1	196.2	-28.3	300	600	
46.93	40.64	37Q1.30	5	9.0	179.4	33.9	250.9	-36.3	237.7	-59.6	300	600	PF1r
47.06	40.76	37Q1.43	5	28.2	175.4	40.7	255.2	-31.5	246.4	-55.8	300	600	
47.87	41.46	37Q2.48	5	11.9	31.7	20.2	13.0	52.1	340.3	49.9	300	600	PF2n
48.57	42.06	38Q1.41	5	2.0	346.3	27.9	104.9	66.3	207.4	83.9	300	600	
50.57	43.80	39Q2.29	5	11.3	32.3	26.6	7.9	54.1	334.6	49.4	300	600	
51.85	44.90	40Q1.65	5	4.2	51.5	1.8	4.0	31.2	348.8	29.0	300	600	
54.20	46.94	42Q2.10	5	2.5	42.8	-2.8	13.2	35.9	353.8	37.0	300	600	
54.89	47.54	43Q1.03	5	3.3	326.5	16.7	127.3	49.5	160.9	65.9	300	600	PF2n
55.91	48.42	44Q2.33	5	10.4	169.8	-6.2	269.0	-56.6	261.9	-82.4	300	600	PF2r
57.29	49.62	46Q1.14	5	23.0	228.3	17.8	194.7	-26.5	180.8	-29.5	300	600	
60.71	52.58	48Q2.53	5	4.3	198.4	23.8	226.7	-39.4	203.3	-54.2	300	600	
61.40	53.17	50Q2.70	5	31.6	189.9	-41.9	209.4	-76.1	124.6	-67.4	300	600	
62.85	54.43	51Q2.15	5	35.3	197.4	-3.1	220.6	-52.8	181.1	-62.1	300	600	
64.71	56.04	52Q2.45	5	13.3	96.1	3.7	335.2	-3.9	339.1	-14.6	300	600	zapped
66.02	57.18	54Q1.19	5	23.0	219.1	18.9	203.1	-31.9	185.2	-37.9	300	600	
66.88	57.92	54Q2.47	5	25.1	74.6	4.9	347.2	14.0	342.6	6.6	300	600	
68.22	59.08	56Q1.25	5	23.0	253.4	25.7	180.8	-5.3	178.6	-4.6	300	600	
68.73	59.52	56Q2.23	5	30.5	285.6	31.9	166.1	22.4	178.0	26.6	300	600	
70.08	60.61	57Q2.47	5	38.9	304.5	7.3	141.9	30.0	158.7	43.5	300	600	
71.37	61.81	59Q1.20	5	8.6	150.6	30.5	283.7	-31.4	290.6	-56.3	300	600	PF2r
72.06	62.41	59Q2.24	5	21.5	116.5	-53.1	358.1	-38.5	17.8	-35.4	300	600	
73.65	63.78	61Q1.44	5	30.8	71.1	46.8	325.4	30.3	317.3	13.5	300	600	
74.25	64.32	63Q1.18	5	24.3	30.8	67.2	297.1	63.2	285.8	38.8	300	600	
75.69	65.549	64Q1.10	5	32.7	351.8	32.4	95.0	71.1	261.2	83.0	300	600	
76.58	66.32	64Q2.28	5	20.1	107.7	59.9	297.5	10.8	297.6	-12.4	300	600	
77.61	67.21	66Q1.35	5	12.2	338.8	30.0	120.5	63.2	190.0	77.1	300	600	PF3n
80.07	69.34	67Q2.67b	5	13.1	346.6	3.4	93.6	54.4	99.4	80.1	300	600	
80.74	69.92	68Q2.05	6	9.8	2.2	9.7	65.8	59.7	10.2	77.4	300	600	

81.60	70.67	69Q1.22	7	11.3	313.0	16.5	139.9	39.5	163.8	52.6	300	600	
85.14	73.73	71Q2.62	6	6.7	336.2	34.8	129.3	63.6	196.5	73.5	300	600	
86.50	74.91	73Q1.22	7	6.8	329.6	26.9	130.5	55.6	175.8	68.9	300	600	
86.83	75.20	73Q2.10	6	3.4	312.4	37.1	154.2	46.0	183.9	51.7	300	600	
89.91	77.86	76Q2.20	6	6.7	18.9	7.6	36.7	54.2	355.6	61.4	300	600	
92.46	80.07	78Q2.13	5	10.3	37.2	5.5	14.9	42.7	350.2	43.4	400	600	
93.85	81.28	79Q2.21	7	6.5	350.5	28.8	96.0	68.5	249.5	85.3	300	600	
94.79	82.09	80Q1.31	6	6.1	344.0	33.6	114.7	68.1	213.9	79.8	300	600	
95.62	82.81	80Q2.37	7	12.6	4.3	51.2	20.9	85.2	282.2	65.4	300	600	
96.40	83.49	81Q2.26	6	8.9	33.1	21.0	10.9	51.4	339.5	48.5	300	600	
97.93	84.81	83Q1.15	7	6.9	20.2	15.5	31.2	57.1	346.8	60.9	300	600	
98.50	85.30	83Q2.22	7	9.9	19.8	5.4	36.2	52.8	357.3	60.2	300	600	
99.90	86.52	84Q2.14	6	8.3	295.4	60.2	187.6	40.0	206.3	32.8	300	600	
103.69	89.80	87Q1.37	7	2.4	332.9	35.5	134.4	61.5	193.3	70.5	300	600	
104.15	90.20	87Q2.20	6	3.6	7.0	8.5	56.7	58.5	4.4	72.8	300	600	
106.88	92.56	89Q1.51	7	7.8	32.4	49.6	340.7	62.5	310.3	46.7	300	600	
107.53	93.12	89Q2.47	7	12.9	354.9	3.1	79.4	56.1	49.8	80.0	300	600	
108.49	93.96	90Q2.15	6	2.2	7.0	3.3	57.6	55.9	12.1	71.6	300	600	
110.62	95.80	92Q1.14	7	13.7	340.4	69.4	218.7	67.3	244.7	46.8	300	600	
112.11	*97.09*	*93Q1.10*	*6*	*20.4*	*356.2*	*4.2*	*77.2*	*56.8*	*41.7*	*79.9*	*300*	*600*	
113.17	98.008	93Q2.40	7	9.7	35.1	15.6	12.0	47.9	343.5	46.3	300	600	
114.39	*99.07*	*94Q2.56*	*6*	*22.8*	*3.2*	*33.5*	*59.8*	*73.0*	*309.8*	*75.8*	*300*	*600*	
115.78	100.27	95Q2.10	7	4.2	348.9	15.6	93.4	61.0	109.5	86.7	300	600	
116.90	101.24	96Q1.22	6	6.8	356.0	39.8	86.9	77.0	275.5	77.1	300	600	
117.43	*101.70*	*97Q1.09*	*7*	*21.4*	*165.4*	*9.3*	*272.2*	*-47.9*	*273.6*	*-73.7*	*300*	*600*	
120.02	103.94	99Q1.09	6	5.3	358.2	30.2	75.5	71.1	305.1	81.0	300	600	
121.16	104.93	100Q2.06	7	11.0	3.8	12.6	62.4	61.1	1.3	76.5	300	600	
123.05	106.56	101Q2.62a	6	6.8	329.7	38.9	142.0	60.5	195.6	66.8	300	600	
123.54	106.99	102Q1.10	6	14.3	1.4	15.4	67.2	62.7	358.1	79.2	400	600	
125.17	*108.40*	*103Q1.51*	*6*	*27.6*	*44.5*	*-0.8*	*10.9*	*35.4*	*352.1*	*35.6*	*300*	*600*	
125.82	108.96	103Q3.11	7	15.9	314.0	47.1	163.5	50.6	196.2	51.3	300	600	
127.44	*110.37*	*104Q2.58*	*6*	*25.5*	*101.2*	*69.2*	*289.7*	*21.2*	*288.5*	*-3.4*	*300*	*600*	
128.03	*110.88*	*105Q1.33*	*7*	*17.5*	*303.0*	*81.3*	*230.6*	*42.9*	*240.3*	*21.7*	*300*	*600*	
128.43	*111.22*	*105Q2.05*	*6*	*31.0*	*338.6*	*33.6*	*124.4*	*64.7*	*198.3*	*75.9*	*300*	*600*	
129.69	112.31	106Q1.46	7	7.7	31.9	4.1	21.2	45.6	352.9	48.4	300	600	
131.44	113.83	107Q2.02	6	6.6	2.8	20.5	63.6	65.4	343.1	78.3	300	600	
133.14	115.30	108Q2.10	7	5.6	309.6	30.6	151.0	41.5	176.8	49.5	300	600	
134.00	116.05	109Q1.20	6	5.4	358.2	13.4	74.0	61.7	11.4	81.8	300	600	
134.68	116.64	109Q2.15	7	5.8	337.1	4.7	108.3	51.0	133.5	74.0	300	600	
		110Q2.13	*6*	*3.8*	*353.3*	*15.0*	*84.4*	*61.9*	*35.3*	*86.1*	*300*	*600*	*ID?*
137.04	118.68	112Q2.05	7	3.9	16.5	-1.6	43.4	50.9	6.5	62.0	300	600	
139.42	120.74	114Q1.06	6	5.9	2.0	28.9	64.5	70.3	318.9	78.2	300	600	
140.10	121.33	114Q2.22	7	4.4	6.2	6.7	58.5	57.8	8.4	73.1	300	600	
141.24	122.32	115Q2.40	6	4.6	10.8	16.5	47.3	61.6	348.6	70.2	300	600	
142.89	123.75	116Q2.59	7	16.2	10.4	13.8	49.0	60.3	353.0	70.4	300	600	PF3n
143.83	*124.56*	*118Q1.12*	*6*	*23.2*	*289.9*	*49.1*	*176.6*	*31.9*	*192.5*	*30.4*	*300*	*600*	
146.70	127.05	120Q2.23	7	15.0	189.2	27.7	238.6	-39.4	217.9	-58.8	300	600	PF3r.1r
147.80	128.00	121Q1.28	6	4.3	195.0	7.0	227.1	-48.9	193.1	-62.1	300	600	
150.00	129.90	122Q2.20	6	2.2	4.3	10.9	61.6	60.1	4.0	75.7	300	600	
153.00	132.50	124Q2.01	6	9.0	183.7	6.4	244.3	-51.5	210.5	-71.1	300	600	
154.43	133.74	125Q2.33	3	12.7	169.3	-11.9	271.4	-59.3	272.4	-85.1	500	600	
155.75	134.88	126Q2.20	6	4.4	191.8	-10.1	227.5	-58.1	177.3	-68.5	300	600	
156.98	135.95	127Q1.63	7	14.6	186.9	18.0	240.5	-45.2	214.5	-64.5	300	600	
157.51	136.41	127Q2.46	6	5.0	207.4	13.7	213.2	-40.7	188.1	-49.6	300	600	
158.60	137.35	128Q2.40	7	2.2	200.1	-3.3	216.5	-51.7	179.1	-59.6	300	600	
159.87	138.45	129Q2.60	6	2.8	180.0	-0.1	250.2	-55.0	212.7	-76.0	300	600	
161.25	*139.65*	*130Q2.55*	*7*	*29.4*	*186.6*	*48.0*	*243.8*	*-25.6*	*233.3*	*-47.5*	*300*	*600*	

162.49	140.72	131Q2.35	6	4.6	179.7	25.5	250.6	-41.5	233.6	-64.4	300	600	
163.34	141.46	132Q1.28	7	14.5	195.9	12.0	227.0	-46.2	196.6	-60.0	300	600	
166.16	143.90	134Q1.05	6	11.7	170.2	-9.2	269.0	-58.2	260.1	-83.9	300	600	PF3r.1r
167.43	145.00	135Q1.10	7	15.6	39.1	62.1	312.8	58.9	296.7	37.1	300	600	PF3r.1n
170.72	147.85	137Q1.35	6	13.7	41.4	33.7	353.7	49.8	328.6	40.6	500	600	PF3r.1n
174.47	151.10	139Q2.34	7	13.3	133.3	-16.8	319.8	-39.8	344.0	-52.9	300	600	PF3r
176.87	153.17	141Q2.31	3	15.8	221.1	4.3	195.4	-36.5	175.3	-38.4	300	500	
177.12	153.39	141Q2.56	5	10.6	160.1	-4.9	284.2	-52.5	307.1	-76.5	500	600	PF3r
177.39	153.62	142Q1.01	6	35.6	249.8	26.1	183.2	-7.9	179.6	-8.0	300	600	
178.21	154.33	142Q2.67	5	8.8	322.2	24.2	136.4	49.2	170.8	61.9	550	675	PF4n
179.93	155.82	144Q1.11	6	28.3	278.3	32.5	170.4	16.7	178.9	19.7	300	600	
181.83	157.47	145Q1.48	7	7.5	0.6	16.3	68.9	63.2	356.7	80.1	300	600	
184.58	159.85	147Q1.18	7	11.6	6.8	18.4	55.0	63.6	346.9	74.3	300	600	
185.69	160.81	148Q2.47	6	14.9	345.4	23.4	103.8	63.6	180.4	84.4	300	600	
186.46	161.48	149Q1.48	7	7.7	332.5	14.9	119.2	52.7	155.7	71.6	300	600	
187.02	161.96	149Q2.34	6	4.9	7.0	4.4	57.5	56.5	10.6	71.9	300	600	
188.64	163.37	150Q3.59	4	8.9	10.5	-0.5	52.4	53.3	11.8	67.6	300	600	
189.11	163.77	151Q1.30	6	14.4	216.2	4.9	200.4	-39.4	177.5	-43.0	300	600	
190.71	165.16	152Q2.52	7	2.5	7.5	17.6	53.7	63.0	348.1	73.5	300	600	
191.67	165.99	153Q2.29	6	19.6	153.8	-30.2	308.0	-59.9	4.2	-72.5	300	600	
193.28	167.39	154Q2.51	7	2.4	358.1	3.8	73.7	56.8	34.0	78.7	300	600	
199.71	172.95	160Q1.08	6	4.8	23.7	5.0	30.9	50.7	355.6	56.4	300	600	
200.93	174.01	161Q2.16	7	32.7	27.5	27.7	12.8	58.0	333.4	54.1	300	600	
203.91	176.59	165Q1.47a	6	30.8	350.7	0.6	86.2	54.1	74.8	79.6	300	600	
203.91	176.59	165Q1.47b	5	10.9	355.8	5.7	78.0	57.5	41.4	80.8	300	600	
205.09	177.61	166Q2.63	7	12.4	6.3	22.5	54.9	65.9	338.4	74.8	300	600	
206.15	178.53	167Q1.72	5	11.5	356.7	28.7	79.5	70.0	304.0	82.7	300	600	
206.48	178.82	167Q2.30	6	38.6	326.8	6.5	121.8	45.7	148.4	65.0	300	600	
207.20	179.44	168Q1.25	4	5.9	352.1	10.8	85.8	59.5	60.6	84.6	200	500	
208.12	180.24	168Q2.46	7	44.1	217.0	4.7	199.5	-39.0	177.0	-42.3	300	600	
208.48	180.55	169Q1.01	6	34.4	305.7	31.6	154.3	38.7	177.5	45.8	300	600	
208.89	180.90	169Q1.42	5	32.0	315.0	29.1	146.0	45.4	175.7	54.8	300	600	
209.18	181.16	169Q2.17	5	14.1	348.0	7.2	92.4	56.6	96.0	82.4	300	600	
209.31	181.27	169Q3.06	7	46.0	314.8	21.4	141.2	42.6	168.0	54.6	300	600	
210.27	182.10	170Q1.27	3	5.6	25.9	30.5	12.5	60.3	330.3	55.5	550	625	PF4n
211.30	182.99	170Q2.62	5	28.5	190.6	46.9	239.8	-26.0	228.1	-46.8	300	600	
212.16	183.74	171Q1.64	6	13.2	74.8	33.2	333.3	22.5	326.9	9.0	300	600	?
222.19	192.42	179Q2.53	5	0.7	196.2	6.4	225.2	-48.8	191.3	-61.2	300	600	PF4r
222.69	192.86	180Q1.20	5	3.7	17.6	14.2	36.0	57.8	349.0	63.4	300	600	
223.56	193.61	180Q2.40	5	10.1	113.0	1.4	325.9	-18.2	336.4	-31.4	300	600	
223.80	193.82	180Q2.64	3	8.3	109.8	4.2	326.8	-14.8	335.7	-27.9	625	675	
224.49	194.41	181Q1.47	3	7.8	154.2	7.2	287.6	-44.3	304.0	-68.1	625	675	
224.87	194.74	181Q2.26	3	10.7	165.7	-28.4	286.5	-66.3	25.9	-83.3	625	675	
236.63	204.93	191Q1.42	3	14.9	203.3	-1.0	213.0	-49.2	179.2	-56.2	500	600	
247.06	213.96	199Q2.02	2	7.7	213.8	-16.2	193.0	-49.1	163.2	-47.6	500	550	PF4r
251.14	217.49	201Q2.49	5	14.2	65.3	-39.3	12.5	5.7	9.0	10.0	300	600	PF5n
252.04	218.27	202Q2.10	5	5.7	30.9	54.2	332.0	64.8	303.8	46.4	300	600	
253.62	219.64	203Q2.25	5	9.8	22.3	10.1	30.6	53.6	351.5	58.4	300	600	
254.52	220.42	204Q1.33	5	5.8	353.5	22.4	85.9	65.8	322.8	87.2	300	600	
255.58	221.34	204Q2.63	5	7.6	328.7	18.6	126.0	51.7	162.9	68.2	300	600	
256.29	221.95	205Q1.58	5	2.9	354.2	9.9	81.6	59.4	43.4	83.4	300	600	
256.58	222.20	205Q2.25	5	4.5	350.9	13.0	88.7	60.3	73.4	85.9	300	600	
257.54	223.04	206Q1.30	5	6.2	285.7	60.4	190.6	33.1	204.8	25.6	300	600	
257.98	223.42	207Q1.13	5	5.9	166.7	-48.3	316.7	-77.4	62.6	-71.0	300	600	zapped?
258.61	223.96	207Q2.38	6	11.5	337.1	13.5	112.3	54.8	149.3	75.9	200	625	
259.91	225.09	208Q1.54	5	3.8	0.1	5.3	70.0	57.6	24.4	77.8	300	600	
259.97	225.14	208Q2.08	5	2.3	4.6	23.3	58.8	66.7	336.2	76.5	300	600	

262.29	227.15	210Q1.17	5	3.8	36.8	6.3	14.9	43.3	349.8	43.8	300	600
263.03	227.79	210Q2.16	5	3.2	359.6	13.6	71.0	61.8	6.7	80.6	300	600
268.53	*232.55*	*214Q1.32*	*5*	*39.9*	*336.3*	*45.0*	*143.9*	*68.0*	*215.0*	*69.0*	*300*	*600*
269.93	233.77	215Q1.20	5	12.1	325.6	7.5	123.5	45.4	150.3	64.0	300	600
271.66	*235.26*	*216Q1.40*	*5*	*25.0*	*293.8*	*35.1*	*163.7*	*30.1*	*180.1*	*34.4*	*300*	*600*
272.10	235.65	216Q2.20	5	14.6	339.6	17.3	110.5	57.8	155.5	78.7	300	625
274.35	237.59	219Q2.07	5	9.6	328.6	30.5	134.6	56.3	181.2	67.6	300	600
278.01	240.76	221Q2.27	5	8.5	351.2	20.1	90.3	64.0	26.1	89.6	300	600

mcd is meters core depth and msd is meters stratigraphic depth of samples (ID) taken in core PFNP-1A that was deviated by 60° from horizontal toward azimuth of 135° in flat-lying strata. N is number of steps between demagnetization temperatures T1 and T2 (°C) used to calculate best-fit magnetization vector described by its maximum angular deviation (MAD), the declination (bDec) and inclination (bInc) in bedding coordinates whose virtual geomagnetic pole is located at longitude (bLon) and latitude (bLat) with respect to present-day coordinates and rotated longitude (rbLon) and latitude (rbLat) with respect to a mean Late Triassic paleomagnetic reference pole for North America (4). Data in italicized red font were rejected for magnetostratigraphic interpretation of polarity; samples with valid data from the tops and bottoms of magnetozones are identified in Notes.

Table S4. U-Pb CA-TIMS zircon dates in upper Chinle Fm.

ID	Unit	mcd	msd	Age Ma	±2s Myr	Ref.
Core PFNP-1A						
52Q2	BFB	64.6	56.0	210.08	0.22	1
158Q2	Sonsela	198.6	172.0	213.55	0.28	1
177Q1	Sonsela	219.4	190.0	212.81	1.25	1
182Q1	Sonsela	225.5	195.3	214.08	0.20	1
Outcrop projected to core PFNP-1A						
BFBo	BFB		56.0	209.93	0.07	2
GPU	Sonsela		172.4	213.12	0.07	2
P57-C	Sonsela		181.0	213.63	0.13	3
KWI	Sonsela		187.4	213.87	0.08	2
GPL	Sonsela		207.8	218.02	0.09	2

Samples (ID) are from lithostratigraphic units in the Chinle Fm. (BFB is Black Forest Bed within the Petrified Forest Mb and Sonsela is Sonsela Mb). Sample levels are in meters core depth (mcd) and meters stratigraphic depth (msd) by accounting for 60° core hole inclination and assuming flat lying strata. The msd for each outcrop sample was projected to core PFNP-1A by correlation of the lithostratigraphy of the measured cumulative section (11, 12) (**Fig. S5**) and registration of the base of the distinctive BFB in outcrop to its equivalent depth in the core. Ref.: 1, This paper; 2, Ref. (11); 3, Ref. (13).

Table S5. Isotopic ratios and ages.

Sample	Pb_c (pg)	Th / U	isotopic ratios: Pb / ^{204}Pb	Pb / ^{206}Pb	2σ %er	Pb / ^{235}U	2σ %er	Pb / ^{238}U	2σ %er	ρ	isotopic age in (Ma): Pb / ^{238}U	
52Q-2.Sp61*	7.2	0.71	114	0.05024	5.22	0.2347	5.46	0.033901	0.54	.49	214.92	± 1.13
52Q-2.Sp314*	1.1	0.51	1242	0.05043	0.54	0.2321	0.65	0.033396	0.29	.56	211.77	± 0.60
52Q-2.Sp115*	1.2	0.99	244	0.05055	2.35	0.2326	2.46	0.033390	0.28	.44	211.73	± 0.57
52Q-2.Sp141*	1.0	1.29	140	0.05026	4.63	0.2311	4.84	0.033370	0.45	.52	211.60	± 0.93
52Q-2.Sp86*	2.1	1.69	61	0.05151	11.39	0.2364	11.90	0.033292	1.14	.49	211.12	± 2.38
52Q-2.Sp201*	0.9	1.65	886	0.05033	0.67	0.2305	0.75	0.033232	0.22	.49	210.75	± 0.46
52Q-2.Sp52*	1.1	0.83	631	0.05054	1.01	0.2312	1.07	0.033197	0.15	.44	210.52	± 0.31
52Q-2.Sp57*	1.2	1.51	247	0.05009	2.38	0.2289	2.50	0.033153	0.33	.42	210.25	± 0.68
52Q-2.Sp108*	0.8	0.59	401	0.04979	1.58	0.2274	1.67	0.033148	0.20	.51	210.22	± 0.41
52Q-2.Sp155*	1.0	0.38	422	0.05060	1.36	0.2311	1.43	0.033137	0.18	.44	210.15	± 0.38
52Q-2.Sp310*	2.0	1.60	63	0.05220	10.69	0.2382	11.17	0.033113	1.07	.49	210.00	± 2.22
52Q-2.Sp204*	1.2	1.25	201	0.04900	3.30	0.2234	3.46	0.033080	0.38	.47	209.80	± 0.79
52Q-2.Sp221*	0.8	1.82	233	0.05017	2.84	0.2285	2.98	0.033043	0.30	.50	209.57	± 0.62
52Q-2.Sp20*	0.9	1.97	234	0.05020	2.66	0.2214	2.81	0.032001	0.35	.46	203.06	± 0.69
158Q-2.Sp60*	3.9	1.50	49	0.05598	14.30	0.2726	14.99	0.035330	1.57	.49	223.82	± 3.46
158Q-2.Sp157*	2.7	1.34	546	0.05069	1.12	0.2410	1.20	0.034500	0.21	.43	218.65	± 0.45
158Q-2.Sp163*	2.7	0.99	1711	0.05038	0.47	0.2385	0.57	0.034346	0.26	.59	217.69	± 0.55
158Q-2.Sp161*	4.7	0.76	341	0.05046	1.80	0.2359	1.91	0.033917	0.27	.45	215.01	± 0.58
158Q-2.Sp181*	4.6	1.41	108	0.04928	11.95	0.2299	12.73	0.033843	1.25	.66	214.56	± 2.64
158Q-2.Sp240*	1.4	1.01	1749	0.05054	0.39	0.2351	0.47	0.033748	0.18	.58	213.96	± 0.38
158Q-2.Sp236*	2.7	1.43	256	0.05114	3.24	0.2377	3.40	0.033730	0.36	.50	213.85	± 0.76
158Q-2.Sp262*	1.2	0.90	1167	0.05018	0.68	0.2330	0.73	0.033696	0.19	.39	213.64	± 0.40
158Q-2.Sp15*	2.0	0.99	370	0.05070	1.52	0.2354	1.60	0.033689	0.22	.42	213.59	± 0.47
158Q-2.Sp93*	1.0	1.36	677	0.05039	0.79	0.2338	0.86	0.033674	0.21	.43	213.50	± 0.43
158Q-2.Sp120*	3.7	1.26	146	0.05062	3.91	0.2347	4.09	0.033647	0.41	.48	213.33	± 0.86
158Q-2.Sp142*	1.4	0.70	1460	0.05064	0.41	0.2344	0.48	0.033583	0.20	.52	212.93	± 0.43
158Q-2.Sp18*	1.3	1.65	127	0.04978	6.86	0.2303	7.24	0.033570	0.72	.57	212.85	± 1.51
158Q-2.Sp233*	1.4	1.34	239	0.04950	4.21	0.2276	4.45	0.033361	0.50	.53	211.55	± 1.04
158Q-2.Sp168*	1.4	1.45	864	0.05058	0.66	0.2297	0.72	0.032954	0.15	.45	209.01	± 0.32
158Q-2.Sp276*	1.1	1.66	1005	0.05015	0.88	0.2268	0.96	0.032816	0.25	.43	208.15	± 0.52
158Q-2.Sp55*	1.7	1.56	686	0.05055	1.18	0.2283	1.26	0.032774	0.23	.43	207.88	± 0.46
177Q-1.Sp181	1.2	1.85	47	0.06067	16.42	0.2856	17.21	0.034134	1.83	.47	216.37	± 3.97
177Q-1.Sp120	1.3	0.71	42	0.05587	19.37	0.2616	20.31	0.033945	2.05	.50	215.19	± 4.40
177Q-1.Sp168	1.2	0.76	445	0.05049	1.37	0.2360	1.44	0.033893	0.20	.42	214.87	± 0.43
177Q-1.Sp108	3.1	0.64	241	0.05066	2.29	0.2357	2.40	0.033748	0.34	.40	213.97	± 0.72
177Q-1.Sp81	1.9	0.76	110	0.05144	5.88	0.2380	6.16	0.033562	0.59	.52	212.81	± 1.25
182Q-1.Sp216	1.6	0.86	194	0.05180	2.86	0.2474	2.98	0.034643	0.30	.45	219.54	± 0.65
182Q-1.Sp273	1.1	0.82	1461	0.05055	0.37	0.2402	0.45	0.034460	0.23	.57	218.40	± 0.50
182Q-1.Sp283	0.6	1.30	439	0.05332	4.03	0.2520	4.35	0.034281	0.79	.48	217.29	± 1.71
182Q-1.Sp269	0.9	1.99	1321	0.05036	0.98	0.2357	1.01	0.033936	0.23	.27	215.14	± 0.50
182Q-1.Sp5	1.1	0.97	574	0.05041	0.91	0.2356	0.99	0.033895	0.28	.40	214.88	± 0.60
182Q-1.Sp266	2.1	0.84	1121	0.05039	0.52	0.2349	1.35	0.033813	1.23	.92	214.37	± 2.64
182Q-1.Sp263	0.7	0.49	1412	0.05026	0.53	0.2343	0.58	0.033810	0.18	.41	214.35	± 0.38
182Q-1.Sp197	0.7	1.05	2330	0.05055	0.34	0.2356	0.45	0.033806	0.26	.64	214.33	± 0.55
182Q-1.Sp241	2.0	0.55	72	0.05349	10.70	0.2492	11.25	0.033789	0.99	.58	214.22	± 2.11
182Q-1.Sp265	0.5	0.52	2178	0.05012	0.35	0.2332	0.41	0.033738	0.18	.54	213.90	± 0.39
182Q-1.Sp182	0.6	0.92	3652	0.05038	0.45	0.2343	0.50	0.033728	0.19	.45	213.84	± 0.41

Pb blank composition is $^{206}Pb/^{204}Pb$ = 18.40 ± 0.64, $^{207}Pb/^{204}Pb$ = 15.64 ± 0.25, $^{208}Pb/^{204}Pb$ = 38.04 ± 0.75, and a $^{206}Pb/^{204}Pb$–$^{207}Pb/^{204}Pb$ correlation of +0.47.
Present day Th/U ratio is calculated from radiogenic $^{208}Pb/^{206}Pb$ and age.
Isotopic ratios corrected for mass fractionation (0.15 ± 0.06%/amu), tracer contribution and common Pb contribution (the latter for all ratios but $^{206}Pb/^{204}Pb$).
ρ is correlation coefficient of radiogenic $^{207}Pb/^{235}U$ versus $^{206}Pb/^{238}U$.
Analyses of aliquotes are printed in grey.
Uncertainties of individual ratios and ages are given at the 2σ level and do not include decay constant errors.
Samples denoted with an * were analyzed using the Earthtime 535 tracer solution.
Deficient radiogenic ^{206}Pb due to initial deficit of ^{230}Th is accounted for by assuming a partition coefficient ratio DTh/DU of 0.2 (as applied in Wotzlaw et al., 2014).
Initial deficit of ^{230}Th for zircons analyzed using ET535 is corrected assuming Th/U=3.5 in the magma.